



Optimal regenerative repair of large segmental bone defect in a goat model with osteoinductive calcium phosphate bioceramic implants

Wei Zhi^{a,1}, Xiaohua Wang^{b,1}, Dong Sun^b, Taijun Chen^a, Bo Yuan^c, Xiangfeng Li^c, Xuening Chen^c, Jianxin Wang^{a,*}, Zhao Xie^{b,**}, Xiangdong Zhu^{c,***}, Kai Zhang^c, Xingdong Zhang^c

^a Key Laboratory of Advanced Technologies of Materials, Ministry of Education, Southwest Jiaotong University, Chengdu, 610031, China

^b Department of Orthopaedics, First Affiliated Hospital, Third Military Medical University (Army Medical University), Gaotanyan No.30, 400038, Chongqing, China

^c National Engineering Research Center for Biomaterials, College of Biomedical Engineering, Sichuan University, Chengdu, 610064, China

ARTICLE INFO

Keywords:

Calcium phosphate bioceramics
Large segmental bone defects
Bone regenerative repair
Osteoinduction
Mechanical stability

ABSTRACT

So far, how to achieve the optimal regenerative repair of large load-bearing bone defects using artificial bone grafts is a huge challenge in clinic. In this study, a strategy of combining osteoinductive biphasic calcium phosphate (BCP) bioceramic scaffolds with intramedullary nail fixation for creating stable osteogenic microenvironment was applied to repair large segmental bone defects (3.0 cm in length) in goat femur model. The material characterization results showed that the BCP scaffold had the initial compressive strength of over 2.0 MPa, and total porosity of 84%. The cell culture experiments demonstrated that the scaffold had the excellent ability to promote the proliferation and osteogenic differentiation of rat bone marrow-derived mesenchymal stem cells (BMSCs). The in vivo results showed that the intramedullary nail fixation maintained the initial stability and structural integrity of the implants at early stage, promoting the osteogenic process both guided and induced by the BCP scaffolds. At 9 months postoperatively, good integration between the implants and host bone was observed, and a large amount of newborn bones formed, accompanying with the degradation of the material. At 18 months postoperatively, almost the complete new bone substitution in the defect area was achieved. The maximum bending strength of the repaired bone defects reached to the 100% of normal femur at 18 months post-surgery. Our results demonstrated the good potential of osteoinductive BCP bioceramics in the regenerative repair of large load-bearing bone defects. The current study could provide an effective method to treat the clinical large segmental bone defects.

1. Introduction

The regeneration and repair of large segmental bone defect is a challenging work in clinical application. There are many factors affecting the treatment effect, including the location and length of the defect, the condition of soft tissue capsule, mechanical environment, age of patients and other related factors, such as metabolic and systemic diseases and related complications [1–4]. So far, there has been no report on synthetic biomaterial that can successfully repair large bone defects without the help of exogenous active factors/cells. This is mainly

because most of the artificial bone products used in clinic use only have osteoconductivity, but no osteoinduction, which makes their comprehensive osteogenic performance unsatisfactory and thus is difficult to achieve the complete new bone regeneration for large segmental bone defect [5–8]. Therefore, it is of great significance to develop artificial bone graft with both good osteoconduction and osteoinduction for clinical repair of large bone defects.

Among the artificial substitutes used for bone defect repair and regeneration, calcium phosphate ceramics are widely regarded as one of the most promising bone substitute materials because their chemical

Peer review under responsibility of KeAi Communications Co., Ltd.

* Corresponding author.

** Corresponding author.

*** Corresponding author.

E-mail addresses: jwang@swjtu.edu.cn (J. Wang), xiezhao54981@163.com (Z. Xie), xzd7303@163.com (X. Zhu).

¹ Those authors contribute equal to this manuscript. E-mail: Wei Zhi: zhiwei@home.swjtu.edu.cn, Xiaohua Wang: wangxiaohua29@163.com

<https://doi.org/10.1016/j.bioactmat.2021.09.024>

Received 4 June 2021; Received in revised form 14 September 2021; Accepted 15 September 2021

Available online 23 September 2021

2452-199X/© 2021 The Authors. Publishing services by Elsevier B.V. on behalf of KeAi Communications Co. Ltd. This is an open access article under the CC

BY-NC-ND license (<http://creativecommons.org/licenses/by-nc-nd/4.0/>).

composition is similar to that of bone, and has good biocompatibility, osteoconduction and osteoinduction [8–13]. Previous studies from our group [11,14,15] and other groups [16,17] have shown that the special phase composition and porous structure of osteoinductive CaP ceramics enable it to interact with signal molecules and extracellular matrix in the host system, thus creating a local environment conducive to new bone formation. Additionally, a large number of studies [18–24] have proved that the process of cell, cell differentiation and osteogenesis during bone induction of calcium phosphate ceramics is consistent with the process of natural bone regeneration or reconstruction from the point of view of histology, material properties and material-body interaction, suggesting that artificial materials themselves can regulate the function of tissue regeneration and guide new bone formation through their own physical and chemical properties. Therefore, by optimizing the physiochemical properties of materials that are closely related to osteoconduction and osteoinduction, it is possible to achieve complete new bone regeneration of large bone defects. However, the design and construction of calcium phosphate ceramic scaffolds with good osteoinductive property and the development of suitable clinical implant devices and implant schemes still be the main challenges for calcium phosphate bioceramics to regenerate and repair large segmental bone defects. For that, in this study we would develop a porous calcium phosphate ceramic scaffold material by means of the optimal design of its morphology and structure based on our research work and establish a goat femoral segmental defect model to investigate the regeneration ability of such calcium phosphate ceramic scaffold and to evaluate its application prospect in the repair of large segmental bone defect (see Scheme 1).

2. Materials and methods

2.1. Preparation and characterization of BCP porous scaffolds

The BCP precursor powder (HA/ β -TCP: 30/70) prepared by wet precipitation method is provided by the National Biomaterials Engineering Research Center (Sichuan University, China). BCP ceramics with

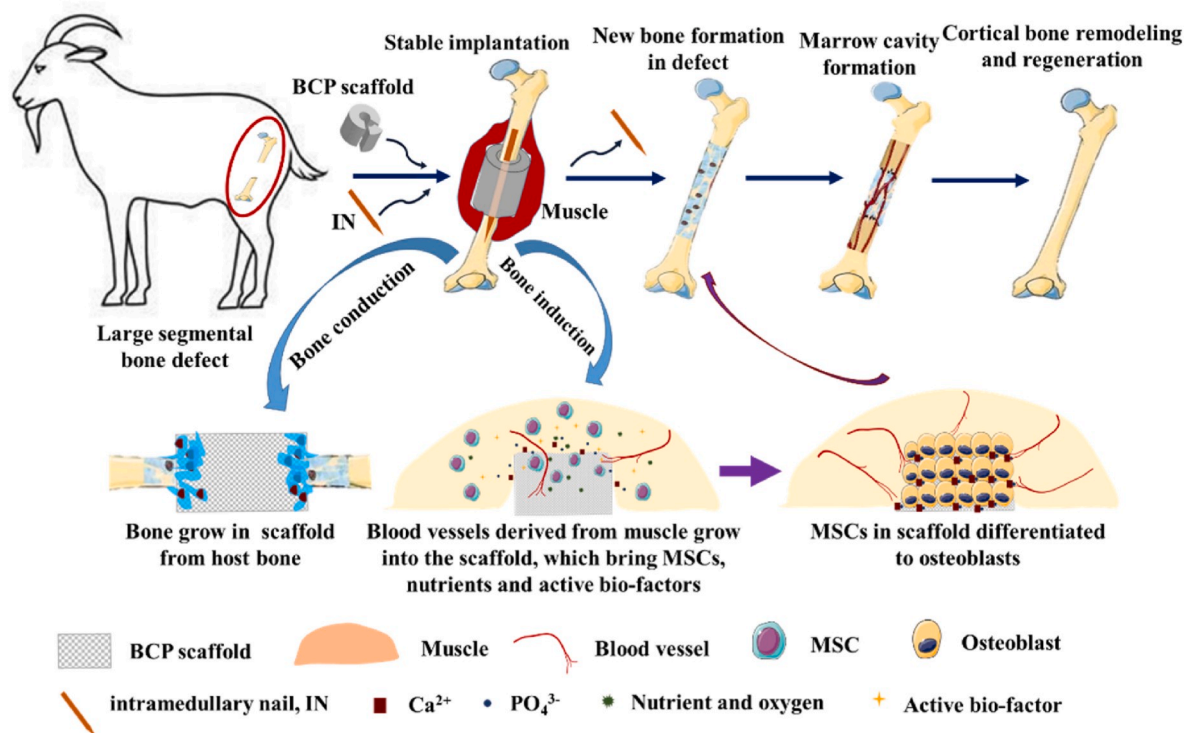
porous structure were prepared by H₂O₂ foaming method [18]: 8 parts of hydrogen peroxide solution, 2 parts of methyl cellulose, 5 parts of polyethylene glycol, 0.2 parts of polyvinyl alcohol and water were added into 20 parts of wet-process apatite powder with a Ca/P ratio of about 1.67. The slurry was prepared according to the ratio of solid to liquid. After stirring in a mixer for about 1 min, the slurry in a mold was heated and foamed in a microwave oven at 2450 Hz and 0.7kw for 1 min, and then dried in an oven at 120 °C for 12 h, and finally sintered in a muffle furnace at 1100 °C for 2 h to obtain calcium phosphate ceramic scaffolds.

The sintered BCP ceramic scaffolds were washed with deionized water, dried at 80 °C for 12 h, and sterilized by γ -ray irradiation. The BCP scaffold was ground into powder and its phase composition was characterized by X-ray diffraction (XRD, Philips, Holland). The micro and macroscopic morphologies of the samples were characterized by scanning electron microscopy (SEM, FEI, USA) and μ -CT (Switzerland SCANCO). The pore structure was characterized by mercury injection method. The compressive strength of scaffolds was carried out using a universal testing machine (Instron-5567Q4052) under environmental conditions. The displacement rate of 0.5 mm/min and five samples were used for testing.

2.2. Osteoinduction evaluation of BCP porous scaffolds in vitro and in vivo

2.2.1. Cell proliferation assay

The 5th generation purified rat bone marrow-derived mesenchymal stem cells were cultured were seeded on the BCP scaffolds at a concentration of 3×10^5 per scaffold in a-Dulbecco's modified Eagle's medium (a-MEM, Gibco, USA) supplemented with 10% fetal goat serum (Excell, China) and 1% penicillin/streptomycin (Gibco, USA) in a humidified atmosphere of 5% CO₂ at 37 °C. at days 1, 3, 7 and 10, the proliferation of BMSCs on scaffolds was analyzed by the Alamar Blue reagent (Invitrogen, USA) cells were incubated with 10% Alamar Blue reagent (5 mL Alamar Blue in 45 mL medium) for 2 h at 37 °C. Next, the



Scheme 1. Schematic diagram of combining osteoinductive biphasic calcium phosphate (BCP) bioceramic scaffolds with intramedullary nail fixation for creating stable osteogenic microenvironment was applied to repair large segmental bone defects (3.0 cm in length) in goat femur model.

media were transferred to a 96-well plate used for measuring the optical density (OD) at 570 nm and 600 nm using a full-wavelength microplate reader (BioTek, USA). Each experiment was carried out in triplicate.

2.2.2. Flow cytometry detection of stem cells specific surface markers

BM-MSCs were seeded on BCP scaffolds and plates, both cultured for 4 days. The cells were trypsinized and centrifuged at 1000 rpm/min for 3 min and then suspended in PBS buffer. After that, they were incubated with stem cells surface marker specific antibodies (FITC-CD 44, BV650-CD90, Bio-Rad, USA) for 30 min, and then rinsed with PBS and centrifuged at 1000 rpm/min for 3 min so as to remove the supernatants. Finally, the cells were analyzed by flow cytometry.

2.2.3. ALP protein analysis

The alkaline phosphate (ALP) activity of BM-MSCs seeded on the scaffolds and plates at 2×10^4 cells/well were detected using ALP quantitative analysis and staining imaging after cultured for 3, 7 and 14 days. The cells were lysed and centrifuged at 12000 rpm/min for 15 min, and the supernatant was detected using alkaline phosphatase assay kit (Beyotime, China) and BCA kit (ThermoFisher Scientific, USA) to determine the ALP activity and the total protein.

2.2.4. Immunofluorescence of bone-specific proteins expression observation

After being cultured for 7 days, immunofluorescence staining of BMSCs seeded on the scaffolds was used to detect the expression of BMP-2, COL-I and OCN. Samples were fixed with 4% paraformaldehyde solution and permeated with 0.5% Triton-X 100. Then, the samples were incubated with primary antibodies at 4 °C for 12 h. After incubation with FITC/APC-conjugated secondary antibody at 37 °C for 1 h, the images were taken by a confocal laser scanning microscope. Then, the bone specific proteins in each sample were quantitatively analyzed via calculating the immunofluorescence density using Image-Pro Plus 6.0 software.

2.2.5. Quantitative real-time polymerase chain reaction (RT-qPCR)

Total mRNA was extracted from BM-MSCs of f-TEB grafts, TEB grafts and control groups with RNA Simple Total RNA kit (Tiangen, China) after cultured for a scheduled time. Then the DNA interference reverse transcription of RNA samples were performed using an iScript™ cDNA synthesis kit (Bio-Rad, USA). RT-qPCR was carried out using iQ™ SYBR® Green supermix (Bio-Rad, USA) via two-step thermochemical cycles at 95 °C for 3 min, followed by 40 cycles at 95 °C for 10 s, 55 °C for 15 s and 72 °C for 30 s, respectively. Melting curves were recorded with continuous fluorescence data acquisition during 65–95 °C melting process. Data were analyzed with the Bio-Rad CFX Manger and each RT-qPCR was performed 3 times. The bone-related specific genes included runt-related transcription factor 2 (Runx2), collagen type I (Col-I), ALP, and osteocalcin (OCN). Glyceraldehyde phosphate dehydrogenase (GAPDH) was selected as the housekeeping gene to normalize the expression levels of target genes and the relative fold change of target gene in each group was calculated using the $\Delta\Delta C_t$ method.

2.2.6. In vivo osteoinduction

Clean grade Chengdu green goats (about 8–12 months) were provided by the Experimental Animal Center of Army Medical University, weighing 23–26 kg, regardless of sex, with a total of 9 goats for 3 different time points. There were 3 parallel BCP samples in each animal. The sample size was $5 \times 5 \times 10$ mm. The operation would be done only in the right limb for each goat. Before operation, the animals that have routinely adapted to the environment (temperature 20–30 °C, humidity 50%–80%) for one week and would be used in the experimental study. The spatium intermuscular between vastus lateralis and vastus intermedius along the muscle fiber direction was bluntly separated to fabricate a muscle package. BCP bioceramic was implanted in the muscle package for 3, 6 and 9 months. The osteoinduction of scaffolds was evaluated using the decalcified samples stained with H&E to

observe osteogenesis and vascularization.

2.3. BCP scaffold design

Considering the strategy of combining scaffolds with intramedullary nail fixation for creating stable osteogenic microenvironment was applied in this study, the material was designed as a C-type hollow cylinder with wedge-shaped trapezoidal side cover closing longitudinally to facilitate implantation and space occupation during operation. Furthermore, the material has an enlarged outer diameter of 30 mm to make it closely surrounded by the surrounding muscle tissue, which prevents displacement of scaffold and is conducive to forming osteoinductive environment, an inner diameter of 11 mm and a length of 26 mm to prevent the material from crushing under positive compression and maintain its integrity (Fig. 1).

2.4. Preparation and postoperative observation of large segmental defect of femur in goat model

All animal experiments are carried out in accordance with the guidelines of the Animal Protection and Utilization Committee of the Chinese institutions. Clean grade Chengdu green goats (about 8–12 months) were provided by the Experimental Animal Center of Army Medical University, weighing 23–26 kg, regardless of sex, with a total of 21 goats for 3 different time points. The operation would be done only in the left limb for each goat. Before operation, the animals that have routinely adapted to the environment (temperature 20–30 °C, humidity 50%–80%) for one week and would be used in the experimental study. According to the anatomical characteristics of goat femur, the interlocking intramedullary nail and supporting internal fixation instruments suitable for goat femur were designed. The intramedullary nail is made of stainless steel, which is solid, with a length of 139 mm and a diameter of 10 mm. The diameter of the interlocking hole is 4 mm, and the central two holes are 70 mm apart. The supporting surgical instruments include sight, guide needle, reaming drill, screw, etc. (all provided by Tianjin Zhengtian Medical equipment Co., Ltd.) (Fig. 2A and B). The operation was performed using the previously reported method. The feeding of the goats was stopped 12 h before operation, the goats were anesthetized by intramuscular injection of Sumianxin (0.15 mL/kg), the right side of the goat was lying on the experimental table, and the skin of the left hind limb was prepared, routinely sterilized and towed. The lateral longitudinal incision of the left femur was taken for about 7 cm to expose the middle part of the femur. A small incision was made to insert the guide needle from the trochanter fossa of the femur, and the hole was reamed with a reaming drill. Under the guidance of the guide needle, the intramedullary nail was inserted into the medullary cavity of the femur, and the guide needle was pulled out through the sight. The guide needle was drilled in both distal end and proximal ends, respectively, and two interlocking screws were screwed in turn. After being examined correctly, the middle part of the femur was sawed off with a wire saw to make the model of 30 mm defect (Fig. 2C). After washing the wound with normal saline, the irradiation sterilized scaffold was implanted into the bone defect (Fig. 2D), sutured layer by layer and bandaged with aseptic dressing, having no external fixation and movement limitation. Penicillin was injected intramuscularly twice a day, 80000 U/time, and streptomycin 0.5 g/d before, during and 3 days after operation. High protein green feed was raised in captivity and stitches were removed 14 days after operation. The general condition and incision healing of goats were observed every day after operation. Gait observation and samples (implanted side and normal side) were taken at 9 months, 12 months and 18 months after operation, and 7 goats were used at each time point.

2.5. Radiographic evaluation

At 9 months, 12 months and 18 months after operation, the animals were killed via excessive anesthetic injection. The bilateral femurs and

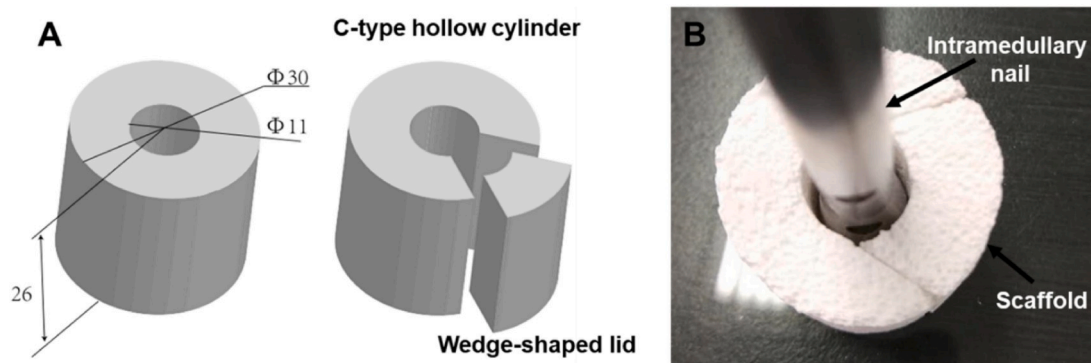


Fig. 1. Shape Design of BCP scaffold. (A) Design drawing of shape parameters of BCP scaffold. (B) The scaffold is matched with the intramedullary nail.

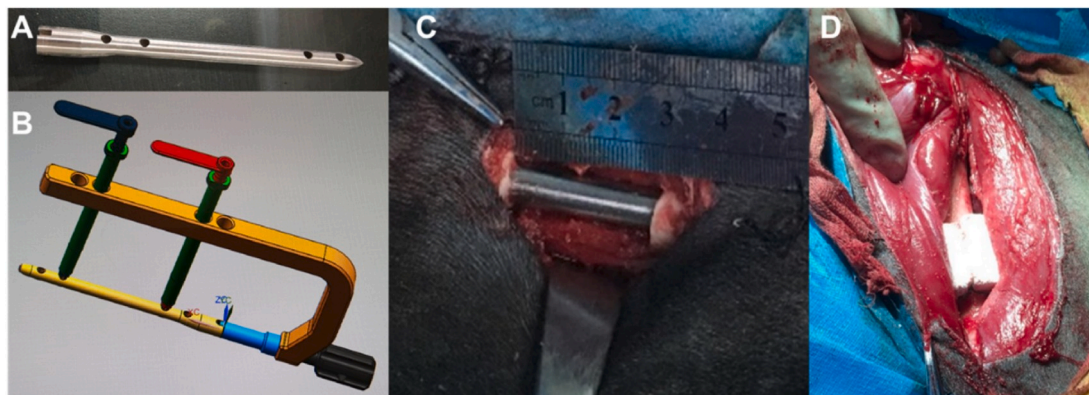


Fig. 2. Preparation of large Segment bone defect Model of Goat femur. (A) Customized intramedullary nail for animal model. (B) Customized auxiliary equipment for implantation operation. (C) Making femur defect model. (D) Scaffold was implanted into the bone defect.

the intramedullary nails were removed from the implanted side successively, and the intramedullary nails were examined by X-ray (the transmission condition was 40 kV 50 mA 0.15 ms). The implants were scored according to the Lane-Sandhu scoring standard (Table 1) by 3 clinicians assessed the X-ray results with a blinded analysis. They were then fixed with 10% formalin solution and then scanned using μ -CT (scanning voltage was 70 kV, current was 113 μ A, 30 μ m/layer), and the bone defect area was reconstructed with the equipment's own software. The threshold of defect was 459mg/cm³ (the amount containing hydroxyapatite per cubic centimeter). 20 random sectional images of each sample at each time point were evaluated visually, the threshold that could best describe the morphology of mineralized tissue was selected, and scaffolds and soft tissues [25] were excluded to determine these indicators. In VOI, the following parameters were measured: bone tissue volume (BV), bone tissue volume/total tissue volume (BV/TV), axial BV distribution, radial bone volume distribution, bone mineral density (BMD) and statistical analysis. The axial BV distribution is evaluated by dividing the total length of the defect into three

equal parts. Two kinds of VOI of Scaffold inner wall (VOI_{inner wall}) and scaffold outer wall (VOI_{scaffold} – VOI_{inner wall}) were used to describe the radial bone volume distribution.

2.6. Biomechanical function evaluation

The samples were collected at 9, 12 and 18 months after operation, respectively, the intramedullary nails, the screws and the soft tissue on the implants were removed, and the external diameter of the implants was measured. The specimens were loaded with 0.5 mm/min on the Instron 5567Q4052 universal mechanical testing machine, and the test distance was 5 cm. The three-point bending test was performed. There were 3 parallel samples in each time point.

2.7. Histological and immune-histochemical tests

The samples were fixed with 4% paraformaldehyde, decalcified in 10% ethylenediamine tetraacetic acid, embedded in paraffin, cut into slices of 5 μ m in thickness and finally stained with hematoxylin-eosin (H&E). Bone immune-histochemical staining was performed using REAL peroxidase/DAB + detection system (Dako, Stockport, UK) and specific mouse primary antibodies. The paraffin-embedded tissue sections were dewaxed in xylene, rehydrated to water through a fractionated alcohol series, air-dried, infiltrated with 0.1% TritonX-100 for 20 min, sealed with 5% goat serum albumin at room temperature for 20 min, and then incubated in an anti-type I collagen (COL-I, AB34710, Abcam, 1:1000) and osteocalcin (OCN, AB13420, Abcam, 1:1000). After washing with PBS, the color was developed with a chromogenic kit. The nuclei were re-stained with hematoxylin and analyzed under light microscope. There were 4 parallel samples for each time point. All specimens were repeated in 5 sections.

Table 1
Lane-Sandhu radiographic scoring standard.

Score	Callus	Fracture line	Bone remodeling
0	No callus	Clear	No bone remodeling
1	Callus occupying 25% of defect	–	–
2	Callus occupying 50% of defect	Partial fracture line	Remodeling of the intramedullary channel
3	Callus occupying 75% of defect	–	–
4	Callus occupying 100% of defect	Completely vanished	Full remodeling of cortex

2.8. Data statistics and processing

In this study, each experimental section was repeated three times, and the result of each study was expressed as mean \pm standard deviation. Students-test was applied to compare between two groups, and one-way analysis of variance (ANOVA) was used for statistical tests for comparison between multiple groups. The difference was considered to be statistically significant when $P < 0.05$.

3. Results

3.1. Preparation and characterization of BCP scaffolds

The surface micro-morphology of calcium phosphate scaffold was observed using a scanning electron microscope, showing that the surface of BCP was rough with a large number of micropores, their size distribution was in the range of 5 μm to 1 mm (Fig. 3A and B). XRD characterization tests show that the material has the HA characterized diffraction peaks at 26°, 32°, 40° and 50°, and β -TCP diffraction peaks at 28° and 34°. The obtained calcium phosphate ceramics belongs to the mixed phase of HA and β -TCP (HA/ β -TCP = 3/7), namely a biphasic calcium phosphate (BCP) (Fig. 3C). The porosity of BCP bioceramic measured was 84%, and the porosity of the interconnected pores was 65%. The average pore diameter was 21.8 μm (Fig. 3D), and the specific surface area was 0.92 m^2/g . The compressive strength of porous bioceramic scaffold was measured to be 2.1 ± 0.1 MPa, which is just in the compressive strength range of 2–12 MPa for cancellous bone, ensuring that the novel scaffold can be used for bone regeneration.

3.2. Osteoinduction characterization

Alamar blue results (Fig. 4A) showed that the proliferation behavior of the cells inoculated on BCP scaffold was obviously enhanced, because the pore structure of the scaffold provided a larger surface area and more space for cell growth. The results of ALP expression detection (Fig. 4B), osteogenic gene qPCR detection (Fig. 4D) and immunocytochemical fluorescence detection (Fig. 4E) showed that BCP scaffold significantly enhanced ALP expression of BMMSC, and up-regulated the expression of osteogenic genes RUNX-2, COL-I, ALP and OCN, as well as the expression of BMP-2, Col-I and OCN. At the same time, the results of flow cytometry detection (Fig. 4C) showed that the expression of CD44 and CD90, the surface stem cell specific markers of BMMSCs on BCP scaffold, decreased from 95.7% to 97.9%–87.7% and 88.5%, respectively, which presented an obvious downward trend, indicating that cells were losing their stem cell characteristics and developed toward differentiation. These in vitro experimental results all confirmed the good osteoinduction of BCP scaffold. Ectopic implantation in vivo showed (Fig. 4F and G) that 3 months after scaffolds implantation, a large number of callus formed in the pores, and new bone grew on the pore wall. 6 months after implantation, a large number of new bones were formed, and then new bones were reconstructed and lamellar bones were formed, accompanied by the growth of blood vessels. After 9 months of implantation, the new bone showed substitutive growth while the scaffold gradually degraded. These results further confirmed the good osteoinduction of the scaffold. There were a lot of new bone tissues in the inner and outer regions of the scaffold, and a trend of material degradation and new bone creeping substitution were observed. The interface between new bone and material has been well integrated. There were a lot of blood

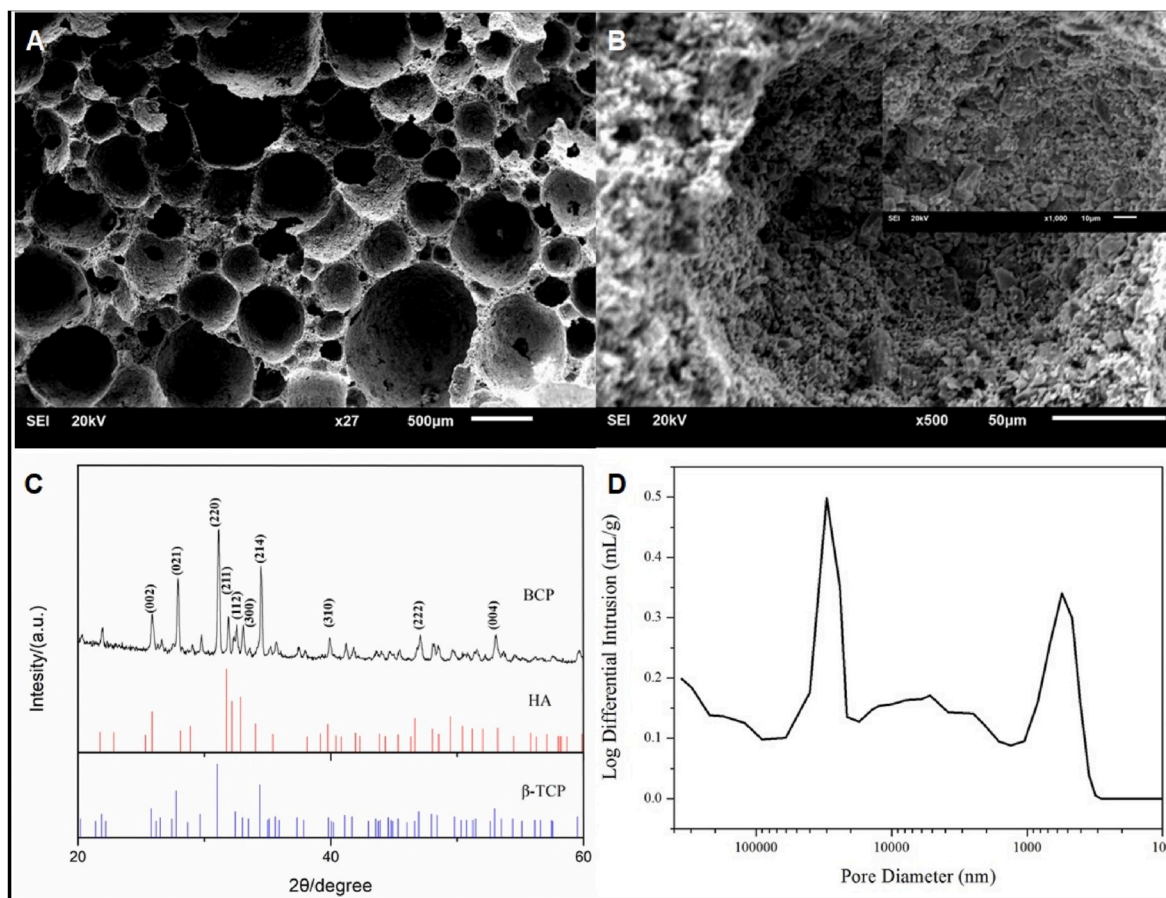


Fig. 3. Characterization of the scaffolds. (A) and (B) The microstructure of the BCP revealed by SEM. The pore size range of the BCP scaffold was in the range of 5 μm to 1 mm (C) XRD patterns of BCP scaffold. (D) Pore size distribution of interconnected pores in BCP scaffold measured by the mercury injection method.

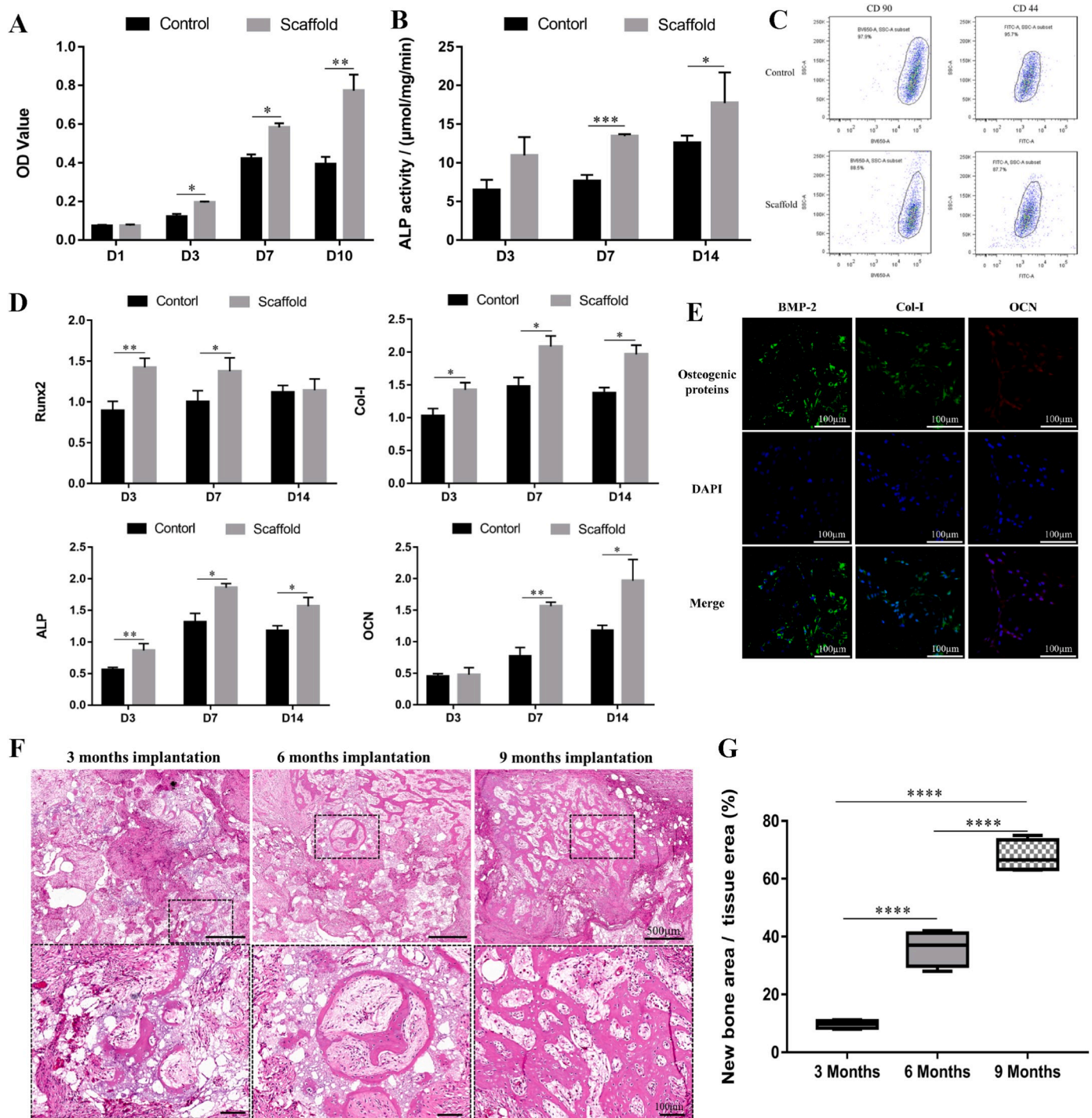


Fig. 4. (A) Cell vitality of BMSCs cultured on BCP scaffolds for 1, 3, 7 and 10 days. The data is expressed as mean ± SD (n = 5). *P < 0.05. (B) The alkaline phosphatase (ALP) activity of BMSCs cultured on plates (Control group), BCP scaffolds for 3, 7 and 14 days. The data is expressed as mean ± SD (n = 3). *P < 0.05, **P < 0.01, ***P < 0.001. (C) The CD 44 and CD 90 expression of BM-MSCs seeded on plates and BCP scaffolds after cultured for 4 days. (D) The expression of Runx2, Col-I, ALP and OCN gene in BM-MSCs of plates (Control group) and BCP scaffolds after 3, 7 and 14 days. The data is expressed as mean ± SD (n = 4) normalized to the expression of GAPDH mRNA. *P < 0.05, **P < 0.01, ***P < 0.001. (E) The expression of BMP-2 (green), Col-I (green), and OCN (red) in BM-MSCs seeded on BCP scaffolds after 10 days. Blue represents the nucleus. Scale bar is 100 µm. (F) HE staining of ectopic osteogenesis after BCP scaffolds after 3 months, 6 months and 9 months implantation in vivo. (G) The percentage of new bone area/total tissue area in H&E staining calculated by Image J software. (One-way ANOVA was used; *p < 0.05; **p < 0.01; ***p < 0.001; ****p < 0.0001).

vessels growing in the scaffold. The new bone center also showed the phenomenon of angiogenesis. The uniform distribution of new bone in the scaffold shows that the high permeability and porosity of the scaffold are beneficial to the growth of new bone in the scaffold.

3.3. Goat model characterization

Adult goats were selected for the study because they had low intrinsic regeneration and similar bone structure to human bone in remodeling, turnover and secondary bone formation. Twenty-one adult

goats were used in this study. A stable 3 cm long defect of the middle and upper femur was made and then the BCP calcium phosphate ceramic scaffold was implanted in the defect. These animals were not fixed after bone defect implantation.

All the animals could wake up 2–6 h after operation and began to drink and eat independently 6 h after operation. The implanted limb could not bear weight just after operation. They could walk with partial weight after 1 week. One month after operation, the implanted limb could walk upright with weight, but had claudication. The gait returned to normal after 3 months. The intramedullary nails of three animals was removed 8 months later, and there was no lameness in walking and running 1 month later (that is 9 months after repair) (Supplementary video), showing that the load-bearing and walking functions of animals have been well restored.

The gross specimens were taken 9 months, 12 months and 18 months after operation, and the results showed that the intramedullary nails were fixed firmly, there was no angular dislocation for implants at the bone defect, and the new bone regeneration and reconstruction were obvious. All animals were in good health and there were no signs of postoperative infection, implant failure or scaffold foreign body reaction.

Compared with the normal femur, the graft material at the femoral defect in the 9-month repair group was well integrated with the host bone, the new bone regeneration and reconstruction at the bone defect were obvious, the diameter of the implant site was significantly thicker, and the bony callus formation was visible to the naked eye. In the 12-month repair group, the new bone regeneration and reconstruction were further strengthened, which were closely connected with the bone end, and the dense bone was visible at the bone defect. In the 18-month repair group, the implant site was more closely connected with the bone end, and the new bone was further reconstructed, and the diameter tended to be similar to the middle and upper part of the normal femur (Fig. 5A).

3.4. Radiographic analysis and biomechanical function evaluation

The X-ray results of 9 months later (Fig. 5B, Fig. S1A) showed the stable bone bonding between the implant material and the host bone. All animals showed the bone formation along the intramedullary nail and the fracture line disappeared. A large number of new bone and bone marrow cavity formation in the defect were observed which showed phenomena of bone remodeling. 3D μ -CT reconstruction showed that some of the defects had been replaced by new bone, while at the defect site, the BCP scaffold had been wrapped by new bone (Fig. 5C). After 12 months, almost most of the defect was filled with new bone, the fracture line disappeared. The characteristic long bone morphology by dense cortical bone and bone marrow cavity composed of cancellous bone has been partially restored (Fig. 5B, Fig. S1B). These 3D μ -CT results were consistent with the results of X-ray, obvious bone remodeling could be seen, and most of the scaffold were degraded (Fig. 6E). After 18 months, most of the defects were replaced by new bone, and the long bone morphology was basically restored (Fig. 5C, Fig. S1C). 3D μ -CT reconstruction showed cortical bone remodeling at 18 months implantation. Sectional images and 3D reconstruction showed that new bone formed and gradually replaced materials after 9 months of BCP scaffold implantation. The replacement was basically completed 12 months after implantation (Fig. 5D). After 9 months of repair, the maximum bending load reached 58% of that of the normal control group, significantly higher after 12 months, reached 79%, and approached the normal bone level after 18 months ($P > 0.05$) (Fig. 5E). The mechanical properties were significantly improved with the increased repair time after scaffold implantation. At the same time, the results also suggest that the repair of mechanical function may mainly occur after the middle stage (12 months) of bone defect repair. The mechanical properties are highly consistent and correlated with the calculated BV, BV distribution, 3D μ -CT reconstruction in the diagram and the macroscopic results in

histological sections. These results further demonstrated that calcium phosphate bioceramic scaffolds without exogenous active factors or cells can treat supercritical large segmental load-bearing bone defects through scaffold-mediated regeneration and mechanical functional reconstruction.

The μ -CT value of the bone volume (BV) of the defect area showed that at 9 months after implantation, the amount of bone formation at the defect was about 70% of the total volume of the defect. After 12 months, the BV/TV reached 90%, and at 18 months, the bone formation at the defect was basically the same as that at 12 months (Fig. 6B). The BMD value of bone mineral density showed that the new bone mineral density at the defect increased gradually with the extension of implantation time, and finally approached the normal bone mineral density (Fig. 6C). By dividing the total length of the defect into three parts of equal length, the axial BV distribution at different repair time points was evaluated. The BV distribution along the z-axis of the defect showed that there was no significant difference in bone formation between the defect/bone interface (Fig. 6D) and the center of the defect at all the time points, but there was a trend of more bone formation in the proximal defect. The results suggested that the vascularization and bone formation of the proximal defect/bone interface are earlier and better than those of the intermediate defect. It is also suggested that the defect regeneration begins at the proximal bone defect and then grows longitudinally along the z-axis of the defect. Macro-CT was used to evaluate the BV of radial bone distribution in the scaffolds, and the scaffold was divided into two parts: the outer wall part and the inner wall part. The results showed that after 9 months, radial bone distribution per unit volume of scaffold outer wall was higher than that of scaffold inner wall, indicating that the new bone growth in scaffold was guided not only from proximal to distal, but also from the outer wall to the inner wall. After 12 and 18 months, the radial bone distribution per unit volume of scaffold was homogeneous, which suggested that the stage of new bone formation had been completed. The results indicated that the uniform distribution of interconnected pores is beneficial to the spatial distribution of new bone in the scaffold (Fig. 6E). According to the standard of radiological scoring of Lane-Sandhu, the scores of the experimental group and the control group were calculated as shown in Table 2. The results suggested that the critical segmental defect of goat femur had been repaired after 18 months implantation of calcium phosphate bioceramic scaffold. The above results show that the highly connectivity of BCP calcium phosphate ceramic scaffold does drive the bone remodeling and the restoration of tubular long bone morphology.

3.5. Histomorphology assessment

The new bone formation, cortical bone reconstruction, medullary cavity recanalization and periosteum regeneration at different repair time points were evaluated by dividing the total length of the defect implantation site into three equal parts. Histological HE staining results (Fig. 7) along Z axis of defect implantation site showed that new bone formation and reconstruction were very active at defect/bone interface (proximal end, distal end) and middle section at all time points, which suggested that the new BCP ceramic scaffold had good bone conductivity so that it could guide the host bone at interface to grow into the defect site. However, the formation of new bone in the middle segment at the same time proved that the scaffold had a good osteoinductive effect, ensured the synchronous regeneration of new bone in the absence of host bone tissue environment, and bridged with the bone tissue growing at both ends. In addition, the bone formation and bone remodeling in the proximal defect/bone interface area are relatively early, suggesting that the conductive growth of bone starts from the proximal defect and then grows downward along the Z axis of the defect. The results showed that after 12 months and 18 months of repair, the bone reconstruction in the lateral area of the scaffold where the defect was implanted was very active, and a large number of lamellar bones and newborn osteon began to appear, and the medullary cavity was

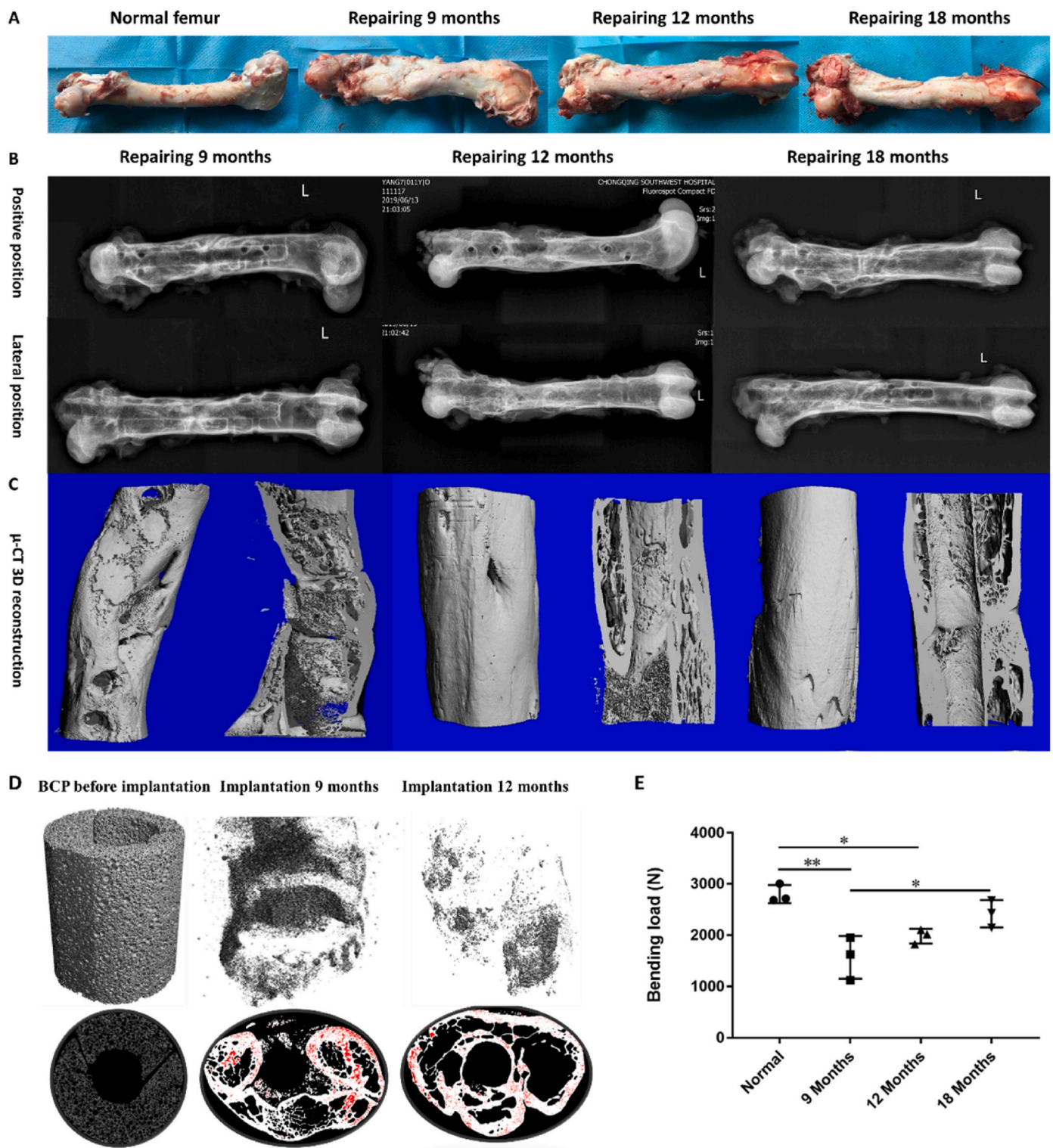


Fig. 5. The gross specimen of goat femur observation (A: Normal femur; B: Implantation 9 months; C: Implantation 12 months; D: Implantation 18 months) and imaging analyses of bone defects after 9, 12 and 18 months. X-ray images and 3D μ -CT reconstructions of samples each time point. (A) The gross observation results showed that the intramedullary nails were fixed firmly, there was no angular dislocation for implants at the bone defect, and the new bone regeneration and reconstruction were obvious. (B) X-ray results showed the stable bone bonding between the implant material and the host bone. Bone formation along the intramedullary nail and disappearance of the fracture line were observed and the characteristic long bone morphology by dense cortical bone and bone marrow cavity composed of cancellous bone has been partially restored at 9 months implantation, and most of the defects were replaced by new bone at 12 months implantation, and the long bone morphology was almost restored at 18 months implantation. (C) 3D μ -CT reconstruction showed part of the defect had been replaced by new bone, while the BCP scaffold had been wrapped by new bone could be seen at 9 months implantation, obvious bone remodeling could be seen at 12 months implantation, and cortical bone remodeling at 18 implantation. (D) Representative tomographic images demonstrating the current working threshold to segment the new bone (grey) from the remaining bioceramic body (red). (E) Biomechanical testing results after 9, 12 and 18 months. Data are median values. Error bars are minimum and maximum values. * $P < 0.05$, ** $P < 0.01$.

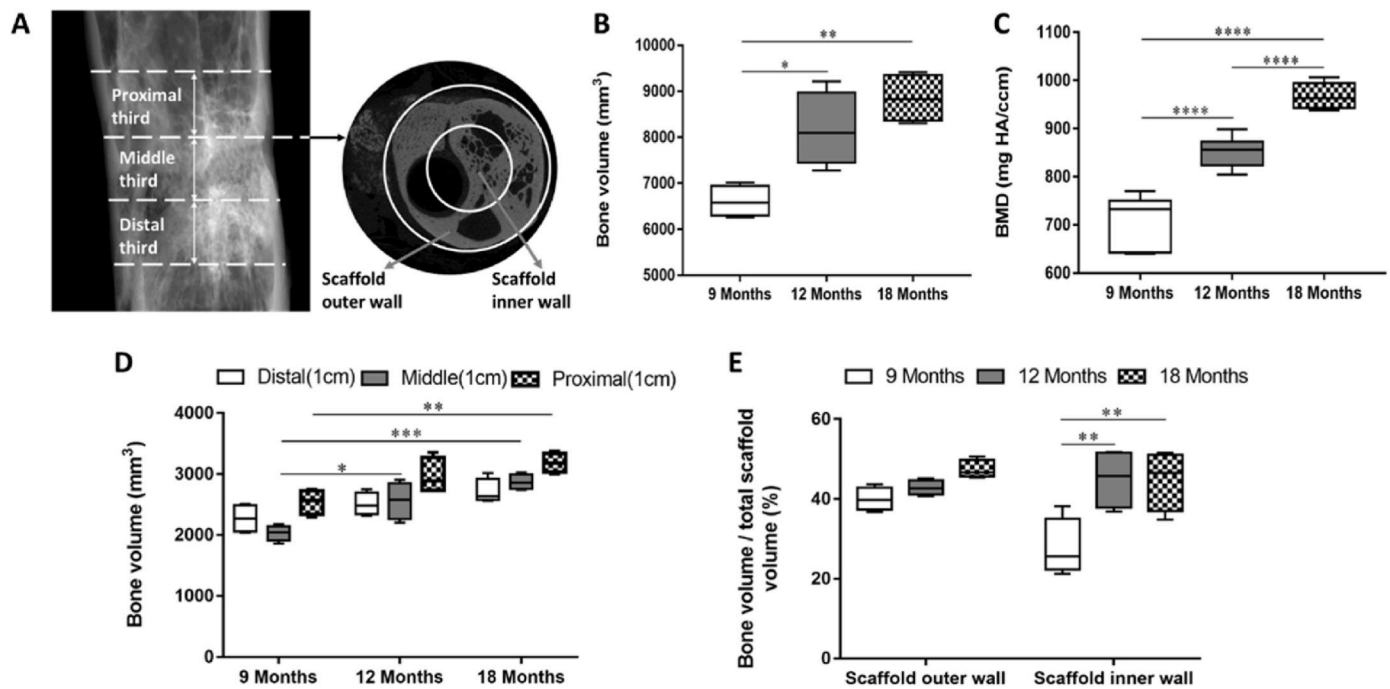


Fig. 6. μ -CT analysis of axial and radial bone distribution after 9, 12 and 18 months. (A) The definition of the VOI is depicted in the 2D longitudinal and transversal μ -CT tomograms. To describe BV distribution along the z axis, the total defect length was divided into three equal thirds (proximal, middle, and distal). The scaffold's inner wall and outer wall characterized radial bone distribution. (B) BVs were calculated as absolute values. (C) Values of median bone mineral density. (D) Axial bone formation in the distal, middle, and proximal thirds in animals. Data are medians \pm minimum and maximum values. (E) Median radial BV in the scaffold's inner wall and its outer wall was normalized as a percentage against the corresponding TV_{scaffold}. Data are medians \pm minimum and maximum values. Error bars are minimum and maximum values. * $p < 0.05$; ** $p < 0.01$; *** $p < 0.001$; **** $p < 0.0001$.

Table 2

The results of radiological scoring of Lane-Sandhu. ($\bar{x} \pm s, n = 7, \text{score}$).

Repairing time	9 months	12 months	18 months
Scores	7.5 \pm 0.52	9.6 \pm 0.52*	11.8 \pm 0.39*

* There were significant differences among the groups ($P < 0.05$).

re canalized. It is suggested that the formation stage of new bone in the scaffold has been completed, which also indicates that the regenerated new bone guided by the scaffold implanted into the defect has begun to have the function of physiological bone.

Furthermore, high-power image observation of histological results of the middle section of repaired femur showed that, after 9 months of repair, the bone defect repair site showed the characteristic of rapid bone growth in the interface area of new fibro-lamellar bone with disorganized collagen fibers (primary callus) and scaffold, as shown in Fig. 8A. Under higher magnification, the vascularized mature bone tissue which contains mineralized bone matrix, unmineralized osteoid, and mature osteocytes in the lacunae (Fig. 8B) was observed. Osteoid was located on the interface of mineralized bone and scaffold (Fig. 8B), which was lined with bone synthetic osteoblasts and bone resorption osteoclasts. The blood vessels in the primary callus and soft tissue were well developed, indicating a good blood supply in the scaffold, which is beneficial to the recruitment of osteogenic-related cells and new bone formation (Fig. 8B). After 12 months, a large number of fibrous lamellar bone at the bone defect site has been replaced by newly formed bone units (Haversian system) (Fig. 8C). The reconstruction of new bone and the combination of woven and lamellar bone can be seen under high magnification, showing the unique morphological characteristics of plexiform bone of sheep bone (Fig. 8D). After 18 months, the reconstruction of secondary bone tissue (bone unit) has been almost completed at the bone defect, and a large number of ordered bone units were distributed around the medullary cavity (Fig. 8E and F). The results

of morphological analysis showed that the new bone formation gradually reached the highest value at 12 months after repair, and then the amount of new bone had not increased significantly (Fig. 8G). This suggests that the repair stage has changed from bone regeneration to bone remodeling, and the complete bone repair was nearly finished. In addition, after 9 months of defect repair, membranous fibrous tissue closely attached to the new bone was observed around the out surface of the implant site, suggesting periosteum regeneration. After 12 months of repair, the membranous fibrous tissue became thicker and denser. The formation of callus can be seen at the junction with new bone. After 18 months of repair, osteoblasts in membranous fibrous tissue were clearly visible, which confirmed the regeneration of periosteum well. Due to the good osteoinduction and osteoconduction of BCP bioceramic implants, after implantation in vivo, they can promote angiogenesis and new bone formation. With the completion of new bone regeneration and reconstruction, periosteum, as an accessory tissue of bone, is thus gradually formed and reconstructed. This phenomenon further confirmed the excellent bone regeneration promoting ability of BCP implants caused by osteoinduction and osteoconduction and illustrates complete bone repair and bone regeneration (Fig. 8H). The results of immunohistochemistry were highly consistent with the results of histological staining (Fig. 8I, J and 8K). There was obvious expression of type I collagen and OCN in the new bone after 9 months, but there was a high expression of OCN in osteocytes in bone units after 12 months, and the expression of both protein markers decreased after 18 months, indicating that matrix calcification was completed in bone remodeling and that osteogenesis and bone remodeling have gradually reached a dynamic balance.

4. Discussion

Calcium phosphate ceramic is considered as the most promising bone substitute material because of its high osteoinduction potential [26–29]. Lots of studies from our group and other groups have proved that the process of cell, cell differentiation and osteogenesis during bone

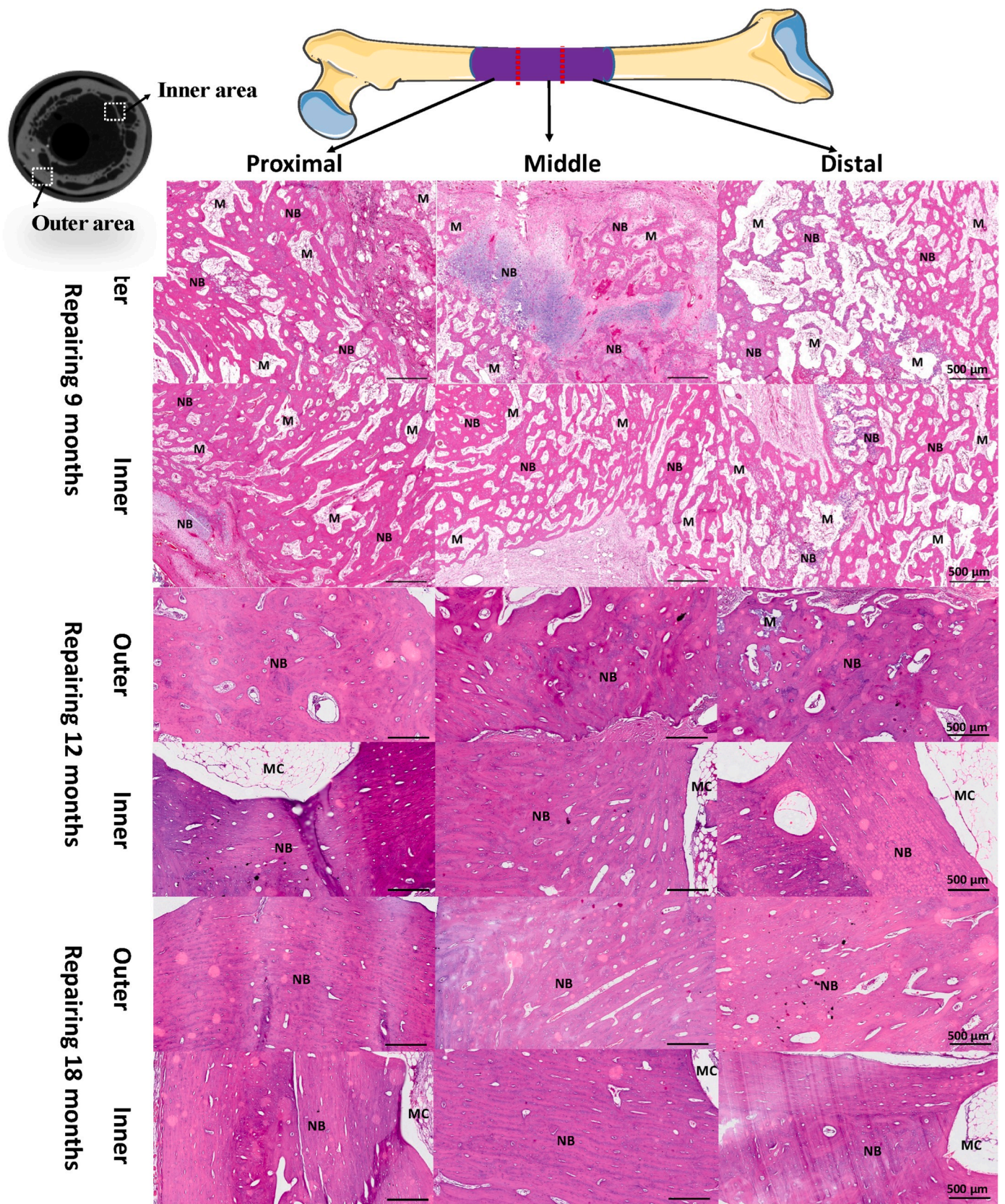
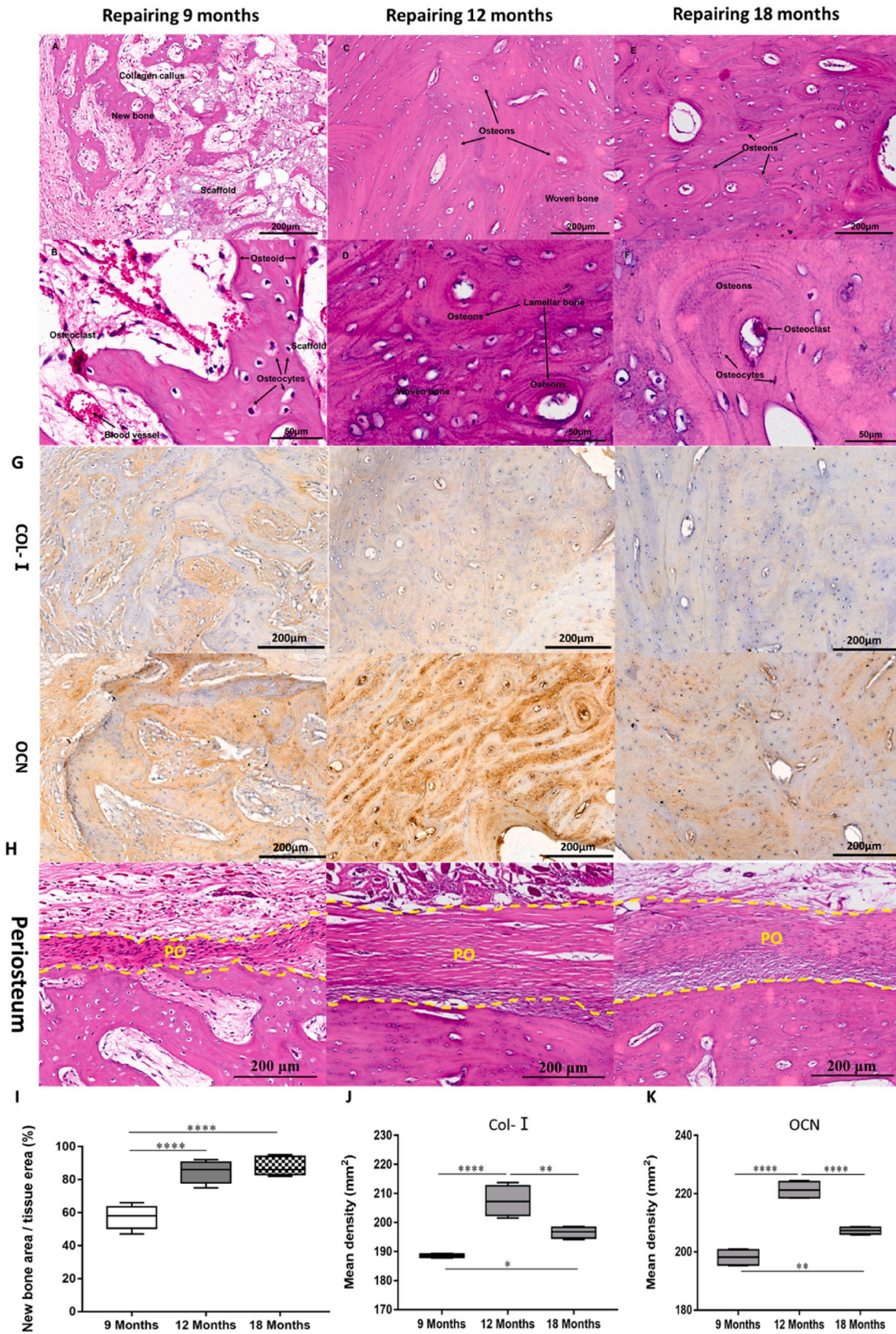


Fig. 7. Histological analysis of the new regenerated tissues in the defect area with the scaffold implantation. Representative HE staining images indicating newly formed tissues including newly mineralized bone tissue (NB), marrow cavity (MC) and BCP scaffolds (M). New bone formation and reconstruction were very active at defect/bone interface (proximal end, distal end) and middle section at all the time points. At 9 months of repair, the formation of new bone in the middle segment and the bone tissue growing which bridged with both ends were observed. The bone formation and reconstruction in the proximal defect/bone interface area were relatively early. At 12 and 18 months of repair, the bone reconstruction in the lateral area of the scaffold where the defect was implanted was very active, a large number of lamellar bones began to appear, and the medullary cavity reconstruction was completed.



(caption on next page)

Fig. 8. Morphology of newly formed bone in BCP scaffold animals from the middle section of repaired femur by random selection. (A to F) H&E and Masson's stain. I Immunofluorescence staining of the decalcified bone slices. After 9 months, the histology sections show the interface among scaffold, new bone and fibrous callus (A) and a higher magnification image of the vascularized mature bone tissue contains mineralized bone matrix, un-mineralized osteoid, and mature osteocytes in the lacunae. Osteoid is located at the junction of mineralized bone and scaffold (B). After 12 months, a large number of fibrous lamellar bone was replaced by newly formed bone units (C). The reconstruction of new bone and the combination of braided bone and lamellar bone can be seen under high magnification (D). After 18 months, the secondary bone tissue reconstruction of the bone defect site has been almost completed, and a large number of ordered bone units are distributed around the medullary cavity (E and F). (G) The results of immunohistochemistry of COL-I and OCN in new bone formation were highly consistent with the results of histological staining. (H) The membranous fibrous tissue between the yellow dotted lines is the regenerated periosteum. (I) The percentage of new bone area/total tissue area in H&E staining calculated by Image J software. (J) and (K) The expression difference of related proteins was quantified. (One-way ANOVA was used; * $p < 0.05$; ** $p < 0.01$; *** $p < 0.001$; **** $p < 0.0001$).

induction of calcium phosphate ceramics is consistent with the process of natural bone regeneration or reconstruction [9,30,31]. However, up to now, there has been no report on synthetic biomaterial that can successfully regenerative repair large segmental load-bearing bone defects without using exogenous active factors or cells. The main reason is that most synthetic biomaterials only have osteoconductive effect, but not osteoinductive effect, thus leading to poor ability in bone formation for middle parts of large segmental bone defects [32,33]. As a result, usually, when new bone has not grown to the middle part of the material, the graft material has fractured due to the decrease of mechanical properties resulting from degradation, whilst osteoinduction is very important for the bone formation of the middle part of the graft material [34–36]. Therefore, the research and development of artificial large segmental bone graft with appropriate initial mechanical strength and both excellent osteoinduction and osteoconduction are of significance for clinical application.

In this study, biphasic calcium phosphate (BCP) bioceramic scaffolds with optimized porosity and interconnectivity and suitable initial compressive were constructed based on our previous researches and technology [14,18,24,37]. In vitro osteoinduction experiment, the results of flow cytometry detection of MSCs specific surface markers showed that the positive proportions of CD90 and CD44 of BM-MSCs in control group were 97.9% and 95.7%, respectively, which were consistent with the expression of specific antigen markers on the surface of BM-MSCs of SD rats reported in the literature [38], demonstrated that the MSCs used in the experiment was a high-purity homogeneous stem cell population. After co-culture of BM-MSCs and BCP scaffolds for 4 days, the expression of surface specific antigen markers has changed, and both surface positive specific antigen markers decreased significantly compared with the control group, indicating that the cells have differentiated. Combined with the significant up regulation of ALP expression and osteogenic gene expression, it can be proved that BCP scaffold regulates osteogenic differentiation. This confirmed the osteoinduction of BCP scaffolds. The results of ectopic implantation in vivo showed active new bone formation and scaffold degradation, which further showed that the BCP scaffold used in this study have good osteoinductive property. Then, the effect of bone defect repair and biological function regeneration of the scaffold was evaluated in a large segmental bone defect model of goat femur. Twenty-one adult goat were selected for the study, mainly considering their similarities with human bone in remodeling, transformation and secondary bone formation [39]. By thoroughly removing the periosteum that surrounds the femur, the inherent regenerative potential of the bone would be further weakened so as to evaluate the ability of bone formation for the grafts better.

The radiological scoring of Lane-Sandhu suggested the large segment femur defect had been completely repaired in clinic. X-ray, Micro-CT analysis and histologic analysis showed that the BCP scaffold successfully not only guided new bone and blood vessels to grow into the scaffold, but also induced waving new bone formation and vascularization, greatly promoted the lamellar bone remodeling and maturation, and finally achieved cortical bone regeneration with Haversian system and periosteum for the defect. The reformation of bone marrow cavity in the implanted grafts at the defect site was observed. This process is similar to the bone osteogenesis and development under physiological condition. Although many studies have shown that new bone formation

occurred in osteoinductive materials in vivo, the subsequent process of maturation and reconstruction of new bone was often overlooked. However, it cannot be considered as a successful bone repair if only the tissue grows into the scaffold without the maturation and reconstruction of bone tissue. The results suggested the BCP scaffolds contributed to the complete recovery of physiological structure of bone. The biomechanical test results showed that the maximum mechanical bending load of the repaired femur reached 79% of the normal femur 12 months after operation, and then reached 100% of the normal value 18 months later, which demonstrated that the BCP scaffold completed the mechanical function regeneration of the large segmental bone defect of femur. Additionally, the performances of the good integration with the proximal and distal host bone and the new bone growth along the BCP scaffold from the end to the center demonstrate the good osteoconduction of BCP scaffold, while the new bone formation in the middle graft showed the excellent osteoinduction, which might be attributed to the scaffold porosity characteristic, which had a total true porosity of 84%, an apparent porosity of 65%, and uniformly distributed interconnected pores.

Studies have shown that the physical and chemical properties of biological calcium phosphate ceramic scaffolds, such as Ca^{2+} and PO_4^{3-} [31], as well as the depression or geometric shape of the pores of the scaffolds [40], provide a necessary osteogenic microenvironment for osteogenesis. Meanwhile, it is found that the pore structure of the material can affect matter transport, cell adhesion, vascularization and bone growth [14,18,40,41]. A basic function of pores in the scaffold is to accommodate the cells that grow into the scaffold while that of the pore connection is to allow body fluids, blood vessels and cells to penetrate into the center of the scaffold and to provide adequate exchange of oxygen and nutrients [42]. So far, almost all the reported osteoinductive materials have interconnected porous structures. Therefore, biological calcium phosphate ceramics with high porosity, interconnection and good osteoinduction are considered to be the prerequisites for successful bone defect regeneration. It is generally believed that the porosity that can be used to repair bone defects ranges from 40% to 80%, which mainly depends on the site of the implant [9]. Furthermore, our previous studies have shown that high interconnected porosity (apparent porosity), compared with those only high true porosity for porous calcium phosphate ceramic scaffolds, can play a significant positive role in promoting both osteoinduction and osteoconduction [25,32,33], which is often overlooked in the study of scaffold design.

Furthermore, micro-CT analysis revealed the degradation rate of the scaffold could match the growth rate of new bone very well. The previous view was that scaffolds should degrade and disappear with the growth of tissues [43,44]. However, the degradation rate of scaffold usually mismatched the maturation and reconstruction of bone tissue growing in it. The rate of scaffold degradation that is faster than that of tissue remodeling and/or maturation will lead to the failure of repair [45,46]. In this study, 12 months after implantation, most of the scaffolds degraded with the secondary remodeling of bone and the formation of bone units, and, after 18 months of implantation, they were almost completely degraded and the implanted site of the defect was almost completely replaced by cortical bone formed after bone reconstruction. The uniform distribution of mature bone tissues and the mechanical stability caused by the complete degradation of the scaffold

finally lead to the regeneration of the mechanical function of the repaired bone defect, which were demonstrated by gait observation and biomechanical function evaluation. These results showed the importance of matching the degradation rate of scaffolds with the rate of new bone formation and remodeling.

Micro-CT results also showed that the novel calcium phosphate ceramic scaffolds could achieve good integration with host bone after 9 months implantation, and the remaining bioceramic body still maintained the general structure of the initial implantation, which suggested suitable load-bearing ability of the scaffold. The initial compressive strength of scaffold determines whether the osteoinduction and osteoconduction of the scaffold can be fully performed after implantation in vivo, and affects the degree of integration between the scaffold and the host bone at the early stage of implantation.

It is well known that the bone formation after calcium phosphate ceramic implantation usually follows the mode of intramembranous osteogenesis, that is, the fibrous tissue is arranged and structured at first, which acted as a secondary supporting network for cells. And then mineralization initiated along the fibrous network, resulting in bone formation and reconstruction to form compact or cancellous bone [4,7,47]. This mode has been widely observed in the histological specimens of this study. Interestingly, endochondral ossification also appeared in the process of bone regeneration in this study (Fig. S2). Endochondral osteogenesis is the osteogenic mode of long bone in osteogenesis and development, and also occurs in the process of bone regeneration of autogenous or allogeneic bone graft implantation. The tissue formed by mesenchymal cells differentiates into chondrocytes and forms cartilage templates. And then the chondrocytes differentiate into hypertrophic chondrocytes. Finally, hypertrophic chondrocytes gradually apoptosis, and their matrix calcification becomes a template for osteoblasts and osteoclasts for bone construction [48,49]. The two kinds of bone formation pathways shown simultaneously by the BCP scaffold proved indirectly that the scaffold with optimized physical and chemical properties had excellent biological activity similar to that of natural bone grafts.

Here, we need to mention although there is no blank control of supercritical large-size segmental bone defect repair, the results of our previous research and related literature show that the middle femur defect of goats exceeding 3 cm cannot be repaired and load-bearing function cannot be restored by itself [39,50], which suggested 3 cm should be the critical size for the repair of segmental bone defect. In addition, these studies found that implantation mode plays a key role in space occupation and mechanical stability of implant graft and host bone. The key to the establishment of large animal bone defect model is to select a suitable internal fixation device. In our previous study [51], we found that the bone marrow cavity of goat femur is thick and the bone skin is thin, hence, it is suitable for intramedullary nail fixation. In order to match the intramedullary nail fixation mode and facilitate implantation, the scaffold is designed as a C-type hollow cylinder with a wedge-shaped strip cover. The C-type hollow cylindrical scaffold is easy to be implanted after the force line is fixed by intramedullary nail, and the wedge-shaped strip cover can effectively maintain the spatial integrity of the combined scaffold. Furthermore, in order to obtain a more stable osteogenic environment, an enlarged outer diameter (3 cm) of scaffold is designed, so that the scaffolds in the implanted site can be firmly wrapped by the muscle tissue to avoid displacement, and has achieved tight interface bonding to facilitate the growth of blood vessels derived from muscle tissue into the scaffold, thus helping interstitial cells, nutrients, active bio-factors and calcium and phosphorus ions to enter the scaffold, which support material-organizational interaction and new bone formation in scaffold. The design strategy provides a guarantee for the treatment of large segmental bone defects, and prove that reliable fixation technique play a key role for the treatment of large segmental bone defects.

Generally speaking, our scaffold design and operation type are successful in the treatment of large segmental bone defects, which will have

a good application prospect for the clinical application in the treatment of large segmental bone defects only using calcium phosphate ceramic scaffolds.

5. Conclusion

In this study, by optimizing the physical and chemical properties of the material, we successfully constructed a calcium phosphate BCP biphasic bioceramic scaffold with both good osteoconductive and osteoinductive abilities, and successfully repaired large segmental goat femur bone defects of more than 3 cm without using exogenous active factors or cells. The results not only emphasized the important role of calcium phosphate bioceramic scaffolds with both good osteoconduction and osteoinduction in bone formation and bone regeneration but also demonstrated the key role of the implantation mode in the space occupying and mechanical stability between the implant and the host bone, which are two essential factors for the successful repair of segmental load-bearing bone defects. Our strategy will provide one idea for clinical repair of large segmental bone defects only by using calcium phosphate bioceramic scaffolds in the future.

Icmje COI statement

None declared.

Ethical review statement

The Ethics Committee of the first affiliated hospital of Army Medical University, PLA approved all protocols.

CRediT authorship contribution statement

Wei Zhi: Data curation, Writing – original draft, preparation. **Xiaohua Wang:** Methodology, Investigation. **Dong Sun:** Visualization. **Taijun Chen:** Data curation. **Bo Yuan:** Software. **Xiangfeng Li:** Formal analysis. **Xuening Chen:** Validation. **Jianxin Wang:** Project administration, Writing – review & editing. **Zhao Xie:** Resources, Writing – review & editing. **Xiangdong Zhu:** Writing – review & editing. **Kai Zhang:** Supervision. **Xingdong Zhang:** Conceptualization.

Declaration of competing interest

The authors declare no competing interests.

Acknowledgments

This work was supported by the National Key R&D Program of China (2016YFC1102000), Research on repair technology and equipment of war injury (AWS17J004-02), and the Science and Technology Innovation Seedling Project of Sichuan Province, China (2021057).

Appendix A. Supplementary data

Supplementary data to this article can be found online at <https://doi.org/10.1016/j.bioactmat.2021.09.024>.

References

- [1] J. Stanovici, et al., Bone regeneration strategies with bone marrow stromal cells in orthopaedic surgery, *Curr. Resear. Transl. Med.* 64 (2) (2016) 83–90.
- [2] H.X. Lin, et al., Research hotspots and trends of bone defects based on Web of Science: a bibliometric analysis, *J. Orthop. Surg. Res.* 15 (1) (2020) 463–480.
- [3] S.D. Schickert, et al., Pre-clinical evaluation of biological bone substitute materials for application in highly loaded skeletal sites, *Biomolecules* 10 (6) (2020) 883–899.
- [4] I. Elgali, et al., Guided bone regeneration: materials and biological mechanisms revisited, *Eur. J. Oral Sci.* 125 (5) (2017) 315–337.

- [5] A. Ho-Shui-Ling, et al., Bone regeneration strategies: engineered scaffolds, bioactive molecules and stem cells current stage and future perspectives, *Biomaterials* 180 (2018) 143–162.
- [6] L. Malladi, A. Mahapatro, A.S. Gomes, Fabrication of magnesium-based metallic scaffolds for bone tissue engineering, *Mater. Technol.* 33 (2) (2018) 173–182.
- [7] B. Lowe, et al., The regenerative applicability of bioactive glass and beta-tricalcium phosphate in bone tissue engineering: a transformation perspective, *J. Funct. Biomater.* 10 (1) (2019) 16–33.
- [8] G.L. Koons, M. Diba, A.G. Mikos, Materials design for bone-tissue engineering, *Nat. Rev. Mater.* 5 (8) (2020) 584–603.
- [9] Z.R. Tang, et al., The material and biological characteristics of osteoinductive calcium phosphate ceramics, *Regener. Biomater.* 5 (1) (2018) 43–59.
- [10] X. Zhang, A Study of Hydroxyapatite Ceramics and its Osteogenesis, *Bioceramics & the Human Body*, 1991, pp. 408–416.
- [11] H.P. Yuan, et al., A preliminary study on osteoinduction of two kinds of calcium phosphate ceramics, *Biomaterials* 20 (19) (1999) 1799–1806.
- [12] M. Chesley, et al., One-step hydrothermal synthesis with in situ milling of biologically relevant hydroxyapatite, *Mater. Sci. Eng. C-Mater. Biol. Appl.* 113 (2020) 110962–110970.
- [13] F.Y. Chen, et al., Effects of hydroxyapatite surface nano/micro-structure on osteoclast formation and activity, *J. Mater. Chem. B* 7 (47) (2019) 7574–7587.
- [14] X.N. Chen, et al., Scaffold structural microenvironmental cues to guide tissue regeneration in bone tissue applications, *Nanomaterials* 8 (11) (2018) 960–974.
- [15] D.Q. Xiao, et al., The role of calcium phosphate surface structure in osteogenesis and the mechanisms involved, *Acta Biomater.* 106 (2020) 22–33.
- [16] H.A. Siddiqui, K.L. Pickering, M.R. Mucalo, A review on the use of hydroxyapatite-carbonaceous structure composites in bone replacement materials for strengthening purposes, *Materials* 11 (10) (2018) 960–968.
- [17] M. Bohner, R.J. Miron, A proposed mechanism for material-induced heterotopic ossification, *Mater. Today* 22 (2019) 132–141.
- [18] Y. Chen, et al., The directional migration and differentiation of mesenchymal stem cells toward vascular endothelial cells stimulated by biphasic calcium phosphate ceramic, *Regener. Biomater.* 5 (3) (2018) 129–139.
- [19] R. Naqshbandi, A. I. Sopyan, Gunawan, Development of porous calcium phosphate bioceramics for bone implant applications: a review, *Recent Pat. Mater. Sci.* 6 (3) (2013) 238–252.
- [20] J.J. Klawitter, et al., An evaluation of bone growth into porous high density polyethylene, *J. Biomed. Mater. Res.* 10 (2) (1976) 311–323.
- [21] F. Bai, et al., The correlation between the internal structure and vascularization of controllable porous bioceramic materials in vivo: a quantitative study, *Tissue Eng.* 16 (12) (2010) 3791–3803.
- [22] R.Z. LeGeros, Calcium phosphate-based osteoinductive materials, *Chem. Rev.* 108 (11) (2008) 4742–4753.
- [23] J. Wang, et al., Fabrication and preliminary evaluation of the osteogenic potential for micro-/nano-structured porous BCP ceramics, *Ceram. Int.* 46 (4) (2020) 4801–4812.
- [24] X.F. Li, et al., Stabilization of Ca-deficient hydroxyapatite in biphasic calcium phosphate ceramics by adding alginate to enhance their biological performances, *J. Mater. Chem. B* 6 (1) (2018) 84–97.
- [25] J.J. Wu, et al., Joint construction of micro-vibration stimulation and BCP scaffolds for enhanced bioactivity and self-adaptability tissue engineered bone grafts, *J. Mater. Chem. B* 8 (19) (2020) 4278–4288.
- [26] N. Eliaz, N. Metoki, Calcium phosphate bioceramics: a review of their history, structure, properties, coating technologies and biomedical applications, *Materials* 10 (4) (2017) 334–437.
- [27] H. Yuan, et al., Osteoinductive ceramics as a synthetic alternative to autologous bone grafting, *Proc. Natl. Acad. Sci. U. S. A* 107 (31) (2010) 13614–13619.
- [28] E. Garcia-Gareta, M.J. Coathup, G.W. Blunn, Osteoinduction of bone grafting materials for bone repair and regeneration, *Bone* 81 (2015) 112–121.
- [29] W. Habraken, et al., Calcium phosphates in biomedical applications: materials for the future? *Mater. Today* 19 (2) (2016) 69–87.
- [30] X.F. Li, et al., Design of hydroxyapatite bioceramics with micro-/nanotopographies to regulate the osteogenic activities of bone morphogenetic protein-2 and bone marrow stromal cells, *Nanoscale* 12 (13) (2020) 7284–7300.
- [31] S. Samavedi, A.R. Whittington, A.S. Goldstein, Calcium phosphate ceramics in bone tissue engineering: a review of properties and their influence on cell behavior, *Acta Biomater.* 9 (9) (2013) 8037–8045.
- [32] J.O. Hollinger, et al., Role of bone substitutes, *Clin. Orthop. Relat. Res.* (324) (1996) 55–65.
- [33] A.J.W. Johnson, B.A. Herschler, A review of the mechanical behavior of CaP and CaP/polymer composites for applications in bone replacement and repair, *Acta Biomater.* 7 (1) (2011) 16–30.
- [34] F.A. Probst, et al., Bone regeneration of minipig mandibular defect by adipose derived mesenchymal stem cells seeded tri-calcium phosphate-poly(D,L-lactide-co-glycolide) scaffolds, *Sci. Rep.* 10 (1) (2020) 2062–2077.
- [35] D.B. Raina, et al., A facile one-stage treatment of critical bone defects using a calcium sulfate/hydroxyapatite biomaterial providing spatiotemporal delivery of bone morphogenetic protein-2 and zoledronic acid, *Sci. Adv.* 6 (48) (2020) eabc1779–eabc1789.
- [36] L. Schroter, et al., Biological and mechanical performance and degradation characteristics of calcium phosphate cements in large animals and humans, *Acta Biomater.* 117 (2020) 1–20.
- [37] J. Wang, et al., Fabrication and preliminary biological evaluation of a highly porous biphasic calcium phosphate scaffold with nano-hydroxyapatite surface coating, *Ceram. Int.* 44 (2) (2018) 1304–1311.
- [38] M. Harting, et al., Immunophenotype characterization of rat mesenchymal stromal cells, *Cytotherapy* 10 (3) (2008) 243–253.
- [39] J.C. Reichert, et al., The challenge of establishing preclinical models for segmental bone defect research, *Biomaterials* 30 (12) (2009) 2149–2163.
- [40] R.A. Perez, G. Mestres, Role of pore size and morphology in musculo-skeletal tissue regeneration, *Mater. Sci. Eng. C-Mater. Biol. Appl.* 61 (2016) 922–939.
- [41] P. Song, et al., Novel 3D porous biocomposite scaffolds fabricated by fused deposition modeling and gas foaming combined technology, *Compos. B Eng.* 152 (2018) 151–159.
- [42] Z.J. Yang, et al., Osteogenic responses to extraskelentially implanted synthetic porous calcium phosphate ceramics: an early stage histomorphological study in dogs, *J. Mater. Sci. Mater. Med.* 8 (11) (1997) 697–701.
- [43] R. Langer, J.P. Vacanti, Tissue engineering, *Science*, *Science* 260 (5110) (1993) 920–926.
- [44] T.S. Karande, J.L. Ong, C.M. Agrawal, Diffusion in musculoskeletal tissue engineering scaffolds: design issues related to porosity, permeability, architecture, and nutrient mixing, *Ann. Biomed. Eng.* 32 (12) (2004) 1728–1743.
- [45] A.G. Mikos, et al., Host response to tissue engineered devices, *Adv. Drug Deliv. Rev.* 33 (1–2) (1998) 111–139.
- [46] P. Felice, et al., Vertical ridge augmentation of the atrophic posterior mandible with interpositional bloc grafts: bone from the iliac crest vs. bovine anorganic bone. Clinical and histological results up to one year after loading from a randomized-controlled clinical trial, *Clin. Oral Implants Res.* 20 (12) (2009) 1386–1393.
- [47] T.A. Einhorn, Enhancement of fracture-healing, *Instr. Course Lect.* 77 (45) (1995) 401–416.
- [48] Q. Lu, X. Lin, L. Yang, Animal Models for Bone Tissue Engineering and Osteoinductive Biomaterial Research, *Racing for the Surface*, 2020, pp. 245–288.
- [49] I. Sallent, et al., The few who made it: commercially and clinically successful innovative bone grafts, *Front. Bioeng. Biotechnol.* 8 (2020) 952–959.
- [50] J.C. Reichert, et al., A tissue engineering solution for segmental defect regeneration in load-bearing long bones, *Sci. Transl. Med.* 4 (141) (2012) 141ra93–141ra102.
- [51] H. Qin, et al., Preparation of animal model of long bone defect used in tissue engineering, *Chin. J. Clin. Rehabil.* 8 (20) (2004) 3974–3975.